AJNR

Enhanced Detection of Diffusion Reductions in Creutzfeldt-Jakob Disease at a Higher B Factor

H. Lee, C. Hoffman, P.B. Kingsley, A. Degnan, O. Cohen and I. Prohovnik

AJNR Am J Neuroradiol published online 12 September 2009
http://www.ajnr.org/content/early/2009/09/12/ajnr.A1756.citation

Published September 12, 2009 as 10.3174/ajnr.A1756

ORIGINAL RESEARCH

Enhanced Detection of Diffusion Reductions in Creutzfeldt-Jakob Disease at a Higher B Factor

H. Lee
C. Hoffman
P.B. Kingsley
A. Degnan
O. Cohen
I. Prohovnik

BACKGROUND AND PURPOSE: Diffusion-weighted imaging (DWI) is sensitive to the cerebral manifestations of human prion diseases. The magnitude of diffusion weighting, termed "b factor," has only been evaluated at the standard $b = 1000$ s/mm^2. This is the first rigorous evaluation of $b = 2000$ s/mm^2 in Creutzfeldt-Jakob Disease (CJD).

MATERIALS AND METHODS: We compared DWI characteristics of 13 patients with CJD and 15 healthy controls at $b = 1000$ s/mm^2 and $b = 2000$ s/mm^2. Apparent diffusion coefficients (ADC) were computed and analyzed for the whole brain by voxel-wise analysis (by SPM5) as well as in anatomically defined volumes of interest (by FSL FIRST).

RESULTS: Measured ADC was significantly lower (by approximately 5%–15%) at $b = 2000$ s/mm^2 than at $b = 1000$ s/mm^2 and significantly lower in patients than in controls. The differences between patients and controls were greater and more extensive at $b = 2000$ s/mm^2 than at $b = 1000$ s/mm^2 in the expected regions (thalamus, putamen, and caudate nucleus).

CONCLUSIONS: Because higher b factors change the absolute value of observed ADC, as well as lesion detection, care should be taken when combining studies using different b factors. While the clinical application of high b factors is currently limited by a low signal intensity–to-noise ratio, it may offer more information in questionable cases, and our results confirm and extend the central role of diffusion imaging in human prion diseases.

Creutzfeldt-Jakob Disease (CJD) is the most notable of human transmissible spongiform encephalopathies. These fatal neurodegenerative conditions are thought to be caused by prions, misfolded proteins devoid of conventional genetic material.[1] The etiology can be infectious, hereditary, sporadic, or iatrogenic; and symptoms primarily include myoclonus, ataxia, and rapidly progressive dementia.[2] Sporadic CJD (sCJD) is the most common subtype of CJD (85%–90%). Familial CJD (fCJD), caused by mutations of the gene encoding the normal form of the prion protein (PrP^c), accounts for approximately 10% of cases worldwide. The most common of these mutations occurs in codon 200 (E200K).

MR imaging has been highly useful for CJD diagnosis, the most sensitive and specific marker being restricted diffusion in the basal ganglia, thalamus, and cortex in diffusion-weighted imaging (DWI).[3,4] DWI can evaluate the microstructure of the brain in vivo by measuring displacement of water molecules for a period of time.[5] The images are constructed by applying a pair of magnetic field gradients for approximately 100 ms; image intensity is then a function of applied gradient amplitude, gradient duration, and diffusion time. In practice, these 3 controlling parameters are combined to derive the so-called b factor. In CJD as well as all other clinical conditions, the vast bulk of studies has been performed at a standard b factor of 1000 s/mm^2. With advancing hardware technology, stronger gradients and faster slew rates have facilitated the use of a high b factor and the ability to obtain images with a greater degree of diffusion weighting. Such high b factor studies have been reported to provide better detection of ischemic stroke, as well as white matter damage in Alzheimer disease and vascular dementia.[6-9] We aimed to evaluate the utility of this technique in CJD.

While DWI images are valuable for clinical diagnosis, their nonquantitative nature limits direct comparison across scans, and their diffusion signal intensity is confounded by transverse relaxation time (T2) effects, complicating interpretation. We, therefore, quantified diffusion by calculating the apparent diffusion coefficient (ADC) and compared the ADC between patients with CJD and matched controls.

Materials and Methods

Subjects

As part of a large prospective imaging study of CJD, both patients and healthy controls underwent DWI scanning at both $b = 1000$ s/mm^2 and $b = 2000$ s/mm^2. Patients all had a clinical diagnosis of probable CJD by World Health Organization criteria,[10] with at least 2 of the following indications: rapidly progressive dementia, myoclonus, visual or cerebellar symptoms, pyramidal or extrapyramidal dysfunction, or akinetic mutism. MR imaging was conducted early in the course of the disease, an average of 3.4 ± 2.3 months from symptomatic onset, prior to the onset of dementia. Because clinical diagnosis at early stages of the disease may be uncertain, all patients (5 sporadic and 8 familial) were followed clinically until death to confirm the diagnosis. They survived 7.1 ± 5.3 months following the MR imaging. Controls were healthy by history, medical and neurologic examination, and neuropsychological testing. As Table 1 shows, healthy subjects were free of cognitive deficits as measured by the Mini-Mental State Examination[11] and neurologic symptoms as measured by the

Received April 23, 2009; accepted after revision May 22.

From the Departments of Psychiatry (H.L., A.D., I.P.) and Radiology (I.P.), Mount Sinai School of Medicine, New York; Departments of Radiology (C.H.) and Neurology (O.C.), Sheba Medical Center, Tel Hashomer, Israel; and Department of Radiology (P.B.K.), North Shore University Hospital, Manhasset, New York.

This work was supported by National Institutes of Health grant RO1 NS43488.

Preliminary account previously presented at: International Society for Magnetic Resonance in Medicine, May 3–9, 2008; Toronto, Ontario, Canada.

Please address correspondence to I. Prohovnik, PhD, Department of Psychiatry, Mount Sinai School of Medicine, One Gustave Levy Pl, New York, NY 10029; e-mail: Isak.Prohovnik@mssm.edu

Indicates open access to non-subscribers at www.ajnr.org

DOI 10.3174/ajnr.A1756

Table 1: Subject characteristics[a]

	Patients	Controls	*P* Value
N	13	15	
Age	59.72 ± 7.72	57.45 ± 10.34	NS
Sex (% male)	62	47	NS
CNS	9.85 ± 3.72	0.33 ± 0.62	<.0001
MMSE	25.22 ± 3.11	28.50 ± 1.62	<.005

Note:—CNS indicates Clinical Neurological Scale; MMS, Mini-Mental State Examination; NS, not significant.
[a] Significant differences between the groups were assessed by *t* test for continuous measures and χ^2 for gender distributions. Symptom severity was quantified by the CNS[12] and MMS.[11]

structured Clinical Neurologic Scale.[12] The patients showed, as expected, significant neurologic symptoms and cognitive deficits, despite their short disease duration. The study was approved by the institutional review board of the Sheba Medical Center, Israel, and the Mount Sinai Medical Center, New York.

Image Acquisition

Scanning was performed at the Sheba Medical Center, Israel, on a 1.5T Signa Excite system (GE Healthcare, Milwaukee, Wisconsin) with a standard quadrature head coil. As part of the standardized study protocol, MR imaging sequences included a single-shot echo-planar spin-echo DWI sequence and a high-resolution anatomical T1-weighted sequence (spoiled gradient-recalled [SPGR]). The SPGR sequence was acquired with 104 contiguous axial sections, FOV = 240 mm, TR = 28 ms, TE = 6 ms, and flip angle = 40°, 1.5-mm section thickness with an acquisition matrix of 256 × 256 yielding reconstructed voxel dimensions of 0.94 × 0.94 × 1.50 mm. Acquisition parameters for DWI with $b = 1000$ s/mm^2 or $b = 2000$ s/mm^2 were identical except for the TE, which was 85 ms for $b = 1000$ s/mm^2 and 100 ms for $b = 2000$ s/mm^2. Forty-eight contiguous axial-oblique sections were acquired with TR = 5000 ms, FOV = 240 mm, 3.0-mm section thickness, and an acquisition matrix of 128 × 128, which was zero-filled to 256 × 256, yielding a reconstructed image resolution of 0.94 × 0.94 × 3.0 mm. Each DWI sequence acquired a non-DWI ($b = 0$ s/mm^2, T2-weighted) and DWIs ($b = 1000$ s/mm^2 and $b = 2000$ s/mm^2), which were derived automatically as a geometric mean of the individual signal intensities (SI) with diffusion gradients along 3 orthogonal directions, $SI_{DWI} = (SI_xSI_ySI_z)^{1/3}$. The $b = 2000$ s/mm^2 scans were always obtained immediately after the $b = 1000$ s/mm^2 scans.

The acquired DWI images were analyzed with Matlab code (MathWorks, Natick, Mass) developed in-house to derive the ADC maps. Parenchymal regions were first delineated by applying the Brain Extraction Tool (BET, Functional Magnetic Resonance of the Brain Software Library [FSL] 4.0, http://www.fmrib.ox.ac.uk/fsl/) onto the $b = 0$ s/mm^2 image. ADC was then calculated by the standard Stejskal-Tanner equation in each voxel,

$$ADC = \ln[S(b1) / S(b2)] / (b2 - b1),$$

where $S(b1)$ and $S(b2)$ are the signal intensities of DWI with applied b factors of $b1 = 0$ s/mm^2 and $b2$, which can be 1000 s/mm^2 or 2000 s/mm^2, respectively.[13] Visual examination of all DWI images was conducted for quality control. Abnormally high signal intensity, in comparison with adjacent sections, was detected in 6 sections (of 2688 sections acquired), 4 in controls and 2 in patients. ADC values were uniformly elevated within these sections and were manually corrected by rescaling to match the intensity of adjacent sections. The artifacts were not spatially selective, and it is not clear whether they were related to a scanner malfunction, bulk head movement, or CSF pulsation.[14-16] Repeated image analysis without these corrections did not alter our results.

Voxel-Wise Image Analysis

Whole-brain voxel-based analyses were performed by statistical parametric mapping (SPM5, Wellcome Department of Imaging Neuroscience, University College London, London, UK). In the spatial processing step, the T2-weighted ($b = 0$ s/mm^2) image was first coregistered with the anatomical image (SPGR), and the resulting coregistration parameters were applied to the ADC map. Normalization parameters were then derived by warping the SPGR T1-weighted image to match the canonical template of ICBM 452 tissue probability maps by using the segmentation approach.[17,18] The resulting normalization parameters were applied onto ADC maps, which were resectioned at 2 × 2 × 2 mm. Last, normalized ADC maps were smoothed by an isotropic 4-mm gaussian smoothing kernel.

The resulting smoothed and normalized ADC images were submitted to a group-level random-effects model of analysis of covariance (ANCOVA) between healthy controls and patients with age as a covariate. We searched for voxels in which the measured ADC was significantly lower in patients with CJD than in controls, with significance thresholds of $P < .001$ (uncorrected) and cluster size, K, greater than 5 contiguous voxels. The nominal $P < .001$ is for 2-tailed tests, yielding an actual significance level of $P < .0005$ for our 1-tailed contrasts. Anatomic locations were identified by Montreal Neurological Institute (MNI) Space Utility ([MSU], http://www.ihb.spb.ru/~pet_lab/MSU/MSUMain.html). A custom explicit mask was also created before statistical analysis to avoid voxels likely to be pure CSF. In each voxel, if any subject's ADC value exceeded the upper limit, 2500 μm^2/s, the voxel was excluded from further analysis.

Volume-of-Interest Analysis

Anatomical volumes of interest (VOI) were identified with FMRIB Integrated Registration and Segmentation Tool (FIRST, FSL 4.0, http://www.fmrib.ox.ac.uk/fsl).[19] Four structures were delineated in bias-field corrected SPGR images: the globus pallidus, putamen, caudate nucleus, and thalamus. On the basis of previous findings,[20,21] we expected the striatum and thalamus to be positive (ie, to show differences between patients and controls), whereas the globus pallidus was expected to serve as a negative control. To calculate mean ADC in each structure, we resectioned the coregistered ADC map to match the image resolution of SPGR by using trilinear interpolation, and masked it by the parcellated images. Voxels classified as a boundary by FIRST (intensity >100) were excluded from the VOI analysis to reduce the risk of including CSF due to a small misregistration between anatomical and diffusion images at tissue-CSF boundaries. Left and right ADC values were averaged and were analyzed by a repeated-measures ANOVA with diagnosis as a grouping factor and the b factor (1000 s/mm^2 versus 2000 s/mm^2) as a repeated measure (age covariance did not change the findings).

Results

The voxel-based SPM analysis between patients and controls at the 2 b factors is depicted in Fig 1 and detailed in Table 2. As expected, ADC was reduced in patients with CJD in deep gray matter structures, specifically the caudate, putamen, and thalamus. The significant clusters with $b = 2000$ s/mm^2 were substantially larger, and the mean differences were greater

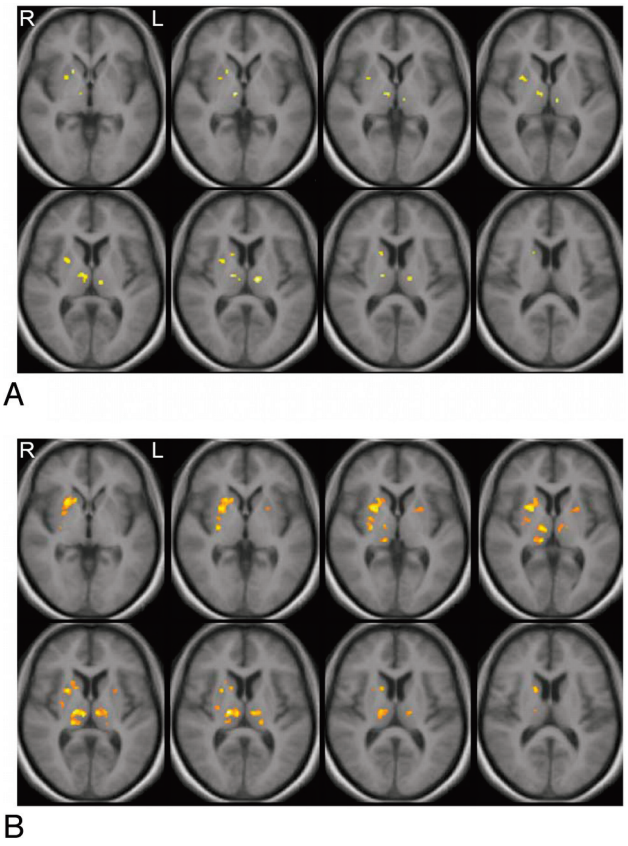

Fig 1. Clusters in which the apparent diffusion coefficient (ADC) was found to be significantly reduced in patients with Creutzfeldt-Jakob disease (CJD) compared with healthy controls at $P < .001$ and $K > 5$. Clusters were overlaid onto averaged T1-weighted images. *A*, Result at $b = 1000$ s/mm^2. *B*, Result at $b = 2000$ s/mm^2. The left and right hemispheres are identified as L and R.

than with $b = 1000$ s/mm^2. For example, the size of clusters occupying the right caudate and putamen increased by more than 5-fold. Furthermore, we observed the emergence of new clusters with the increase in b factor; unilateral findings in the right putamen at 1000 s/mm^2 became bilateral at 2000 s/mm^2. The pulvinar was also involved as a part of a large cluster found in the thalamus with $b = 2000$ s/mm^2. ADC images of an individual patient (case 2018) at both b factors are illustrated in Fig 2.

ADC was also analyzed with repeated-measures ANOVA within each of the parcellated anatomical VOIs. The main effect of the b factor was highly significant ($P < .0001$ in all structures, including globus pallidus), with ADC lower at the higher b factor. The main effect of the diagnosis was significant (ADC was lower in patients) in the putamen ($F_{1,26} = 5.44$, $P < .03$), caudate ($F_{1,26} = 82.78$, $P < .001$), and thalamus ($F_{1,26} = 6.56$, $P < .02$), but not in the globus pallidus. Additionally, in the caudate ($P < .01$) and thalamus ($P < .01$), there was a significant interaction between the b factor and diagnostic group, indicating that the differences between patients and controls were greater at $b = 2000$ s/mm^2 than at $b = 1000$ s/mm^2.

These results are summarized in Fig 3. While ADC was always lower at $b = 2000$ s/mm^2 than at $b = 1000$ s/mm^2, these differences were larger in patients than in controls: caudate (13% versus 7%), putamen (8% versus 4%), thalamus (15% versus 10%), and globus pallidus (13% versus 11%). Consequently, the differences between patients and controls were larger at $b = 2000$ s/mm^2 (8%–11% in the caudate, putamen, and thalamus) than at $b = 1000$ s/mm^2 (3% ~ 8%). The globus pallidus, as expected, showed the smallest diagnostic effect (1% at $b = 1000$ s/mm^2, 3% at $b = 2000$ s/mm^2).

Discussion

DWI is known to provide a sensitive diagnostic test for CJD.[4,22] Previous studies have all been conducted at the standard b factor of 1000 s/mm^2; this is the first quantitative study of DWI at $b = 2000$ s/mm^2 in human prion diseases, and our results demonstrate that a higher b factor yields a better discrimination of patients with CJD from controls. The magnitude of our ADC reductions in patients with CJD at the conventional $b = 1000$ s/mm^2 is also consistent with that in previous reports. Our current results in patients with early CJD show 3%–8% ADC reductions in the anatomically defined basal ganglia and thalamus and 11%–15% in the clusters defined by the voxel-based analysis. Lin et al (2006)[23] reported an average reduction of 14% in ADC in the caudate, thalamus, putamen, and cortical areas. Others reported thalamic reductions of 17% and larger effects in the putamen (22%) and caudate nucleus (29%).[24] We found similar reductions in a preliminary report on patients with fCJD with the E200K mutation.[25]

Voxel-wise analysis revealed unilateral and bilateral ADC reductions in the putamen at $b = 1000$ s/mm^2 and $b = 2000$ s/mm^2, respectively. Case reports have previously described unilateral signal-intensity abnormalities in MR imaging of patients with CJD, but studies with larger samples consistently showed bilateral involvement.[24-31] In the current study, we have confirmed bilaterally reduced ADC in the putamen at $b = 1000$ s/mm^2 with a more liberal statistical significance level ($P < .005$). We believe the absence of bilateral findings in the putamen at $b = 1000$ s/mm^2 merely reflects its lower statistical power.

Contrary to other diffusion studies in CJD, which were based on visual ratings, our quantitative voxel-wise analysis failed to detect significant cortical involvement, often described as cortical ribbons. To explain this, methodologic aspects as well as sample demographics should be considered. In uncontrolled studies, cortical hyperintensities, usually in the cingulate gyrus and insular regions, may represent false-positive findings, because they are also common among neurologically healthy subjects. Asao et al (2008),[32] for example, observed that most DWI images of healthy subjects appear hyperintense in the cingulate gyrus and insula. Also, cortical diffusion abnormalities in CJD are focal and sparsely distributed, often in variable locations across individual patients.[33] These are efficiently detected by visual examination of images, but lesions must be overlapping at the spatial resolution of voxels to be detectible by voxel-wise analysis. Such overlap may be rare in prion diseases, where the precise location of cortical involvement is variable. Additionally, the differential involvement of the cortex and basal ganglia may depend on molecular subtypes of methionine/valine polymorphism at codon 129 of the prion protein gene (*MM, MV, VV*) as well as on the duration of the disease,[34-36] and possibly the

Table 2: Summary of clusters in which ADC was found to be significantly reduced ($P < .001$) among patients compared with normal controls[a]

MNI (x,y,z)	K	*t*	Controls Mean	Controls SD	Patients Mean	Patients SD	% Difference	Anatomical Locations	Side
$b = 1000$									
(−12,−16,8)	20	4.96	777	45	684	63	12	Thalamus (medial dorsal nucleus, ventral lateral nucleus, ventral posterior lateral nucleus)	L
(10,−12,0)	30	4.90	769	40	683	60	11	Thalamus (medial dorsal nucleus, ventral lateral nucleus)	R
(18,12,−2)	6	4.47	782	68	670	76	14	Caudate body, caudate head, putamen	R
(24,4, −4)	31	4.24	725	46	613	80	15	Putamen	R
(16,10,10)	6	4.12	746	58	632	96	15	Caudate body	R
$b = 2000$									
(16,−16,8)	121	6.37	722	40	624	70	13	Thalamus (medial dorsal nucleus, ventral lateral nucleus, ventral posterior lateral nucleus, pulvinar)	R
(26,6,2)	195	5.67	706	35	582	77	17	Caudate body, caudate head, putamen	R
(28,−14,2)	38	5.27	702	37	593	82	15	Putamen	R
(−6,−16,6)	43	5.05	700	35	607	67	13	Thalamus (medial dorsal nucleus, ventral lateral nucleus, ventral posterior lateral nucleus, ventral posterior medial nucleus)	L
(−16,−26,8)	6	4.27	737	59	641	80	13	Pulvinar	L
(−24,6,4)	20	3.87	712	40	585	123	18	Putamen	L

Note:—ADC indicates apparent diffusion coefficient; MNI (x,y,z), Montreal Neurological Institute coordinates of voxel at a peak *t* value; K, size of clusters in the unit of voxels; *t*, corresponding *t* value of a peak height.
[a] Mean and SD were computed within each cluster. Percentage difference is defined by taking the ratio between mean ADC of patients and controls. The left and right hemisphere are identified as L and R.

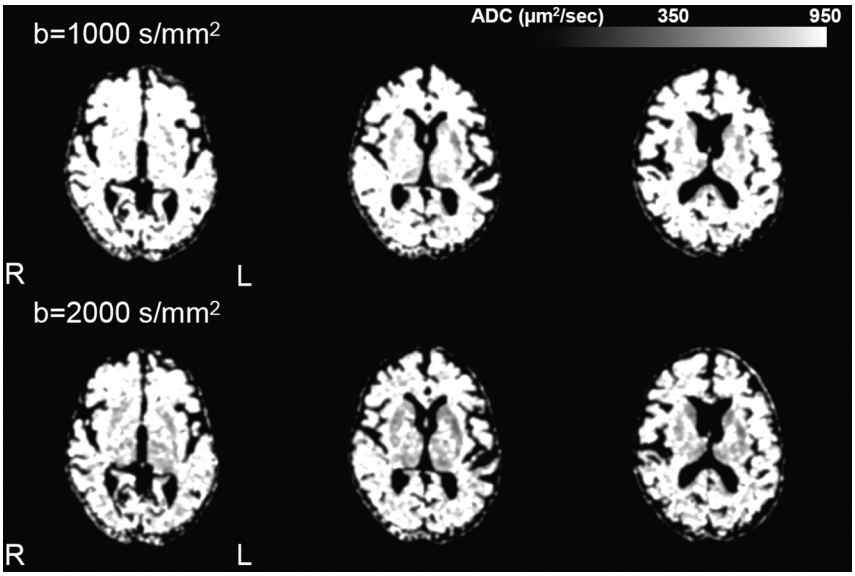

Fig 2. Representative ADC maps of a patient with sporadic CJD (sCJD) (case 2018) at $b = 1000$ s/mm^2 and $b = 2000$ s/mm^2. For illustration purposes, images were smoothed with a 3-mm isotropic smoothing kernel. Signal-intensity abnormality involves the caudate, putamen, and thalamus bilaterally and becomes more extensive at $b = 2000$ s/mm^2 compared with b=1000 s/mm^2. The left and right hemispheres are identified as L and R.

clinical phenotype. An examination of this heterogeneity should be pursued in future work.

Our findings reinforce the current notion that diffusion MR imaging reveals processes fundamental to prion disease, because greater diffusion-weighting increases diagnostic discrimination. The reason for improved discrimination at a higher b factor is unknown, but we hypothesize that it is due to an interaction between prolonged diffusion length at a high b factor and CJD-specific histopathology. The relationship between diffusion abnormalities and histopathology has only been studied in a few case reports and is not yet clear. Diffusion-weighted signal-intensity changes are variably associated with all the hallmarks of CJD histopathology, spongiosis, gliosis, prion protein (PrP^{Sc}) deposition, and neuronal loss; and we believe the major cause of diffusion changes involving both hindered and restricted diffusion components is primarily due to the presence of vacuoles (and, possibly, prion deposits).[37] This idea is based on theoretic considerations and some empiric support based on postmortem studies.[38,39] A similar effect of hindered diffusion was observed for amyloid deposits in transgenic mice, supporting this notion.[40]

Methodologically, our findings underscore the possible

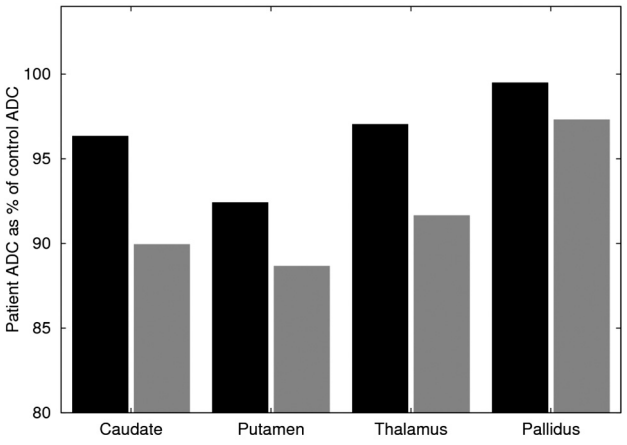

ADC (μm²/sec)	Caudate	Putamen	Thalamus	Globus pallidus
Controls at b=1000	822 ± 53	739 ± 35	848 ± 46	798 ± 44
Patients at b=1000	792 ± 100	683 ± 82	823 ± 57	794 ± 48
Controls at b=2000	766 ± 30	706 ± 27	767 ± 34	710 ± 39
Patients at b=2000	689 ± 72	626 ± 94	703 ± 57	691 ± 66

Fig 3. Bar graphs ($b = 1000$ s/mm^2 in black, $b = 2000$ s/mm^2 in gray) depict the patient ADC as a percentage of the control ADC. Mean ± SD ADC values are listed in the table for each structure.

hazards of combining diffusion data obtained at different b factors, now that this technology is more widely available. ADC is sometimes considered a stable and quantitative tissue parameter, a notion that seems to be contradicted by our finding of a lower ADC at a higher b factor. However, this is fully consistent with previous literature and explained by the multiexponential nature of diffusion-weighted signals. Standard DWI methods assume monoexponential diffusion signal-intensity decay as a function of the b factor, but there is a strong basis to assume that signal-intensity decay is at least biexponential at high b factors, though the mechanism of the multiexponential signal-intensity decay is still under debate.[41-45] In the biexponential model, the diffusion signal intensity at a given b factor is proportional to the sum of fast and slow diffusion components; at a low b factor, much of the ADC signal intensity is contributed from the fast component, whereas at a high b factor, the signal intensity is dominated by the slow diffusion component, lowering ADC. Previous work in healthy subjects suggested 8%–14% reductions of ADC at $b = 2000$ s/mm^2, compared with $b = 1000$ s/mm^2.[41,46] Our finding of 4%–11% reductions is consistent with these reports. While the current findings should encourage and validate the use of higher b factors in diffusion studies of prion disease, combining variable b factors, such as in the work of Meissner et al,[35] may lead to erroneous conclusions. At the very least, if studies include scans obtained at different b factors, this confounding ADC reduction should be statistically controlled and accounted for and the results cautiously interpreted.

The clinical utility of a higher b factor in human prion diseases should ultimately be assessed by blind controlled studies that will quantify diagnostic sensitivity and specificity. Currently, we believe the clinical utility of a high b factor DWI is limited by a suboptimal signal intensity–to-noise ratio (SNR). Figure 4 illustrates this consideration by depicting DWI images of 2 patients with fCJD and 2 patients with sCJD,

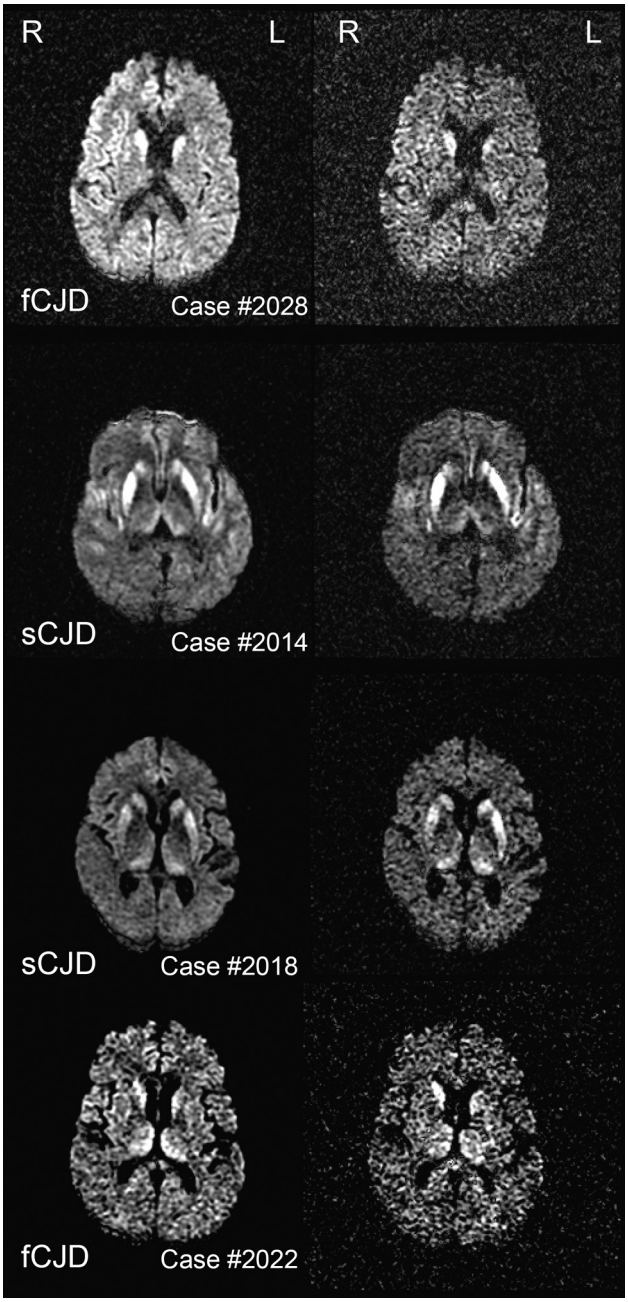

Fig 4. Representative imaging findings on diffusion-weighted imaging at $b = 1000$ s/mm^2 and $b = 2000$ s/mm^2 sequences in 4 symptomatic patients (2 with familial CJD [fCJD] and 2 with sCJD). Signal-intensity abnormalities involve the caudate nucleus, putamen, thalamus, and cortex. The left and right hemispheres are identified as L and R.

showing hyperintense lesions in the caudate nucleus, putamen, thalamus, and cortex. Because DWI signals attenuate exponentially with respect to the b factor, images acquired at $b = 2000$ s/mm^2 become inevitably noisier than those at $b = 1000$ s/mm^2, and precise anatomy is more difficult to ascertain. The combination of higher lesion detection and lower SNR suggests that further optimization of high b factor imaging (eg, by considering high-field scanning, signal intensity averaging, parallel imaging, and reducing the TE) may offer greater diagnostic accuracy in the future.

Acknowledgments

We thank the Wellcome Trust Centre for Neuroimaging at University College London (http://www.fil.ion.ucl.ac.uk/spm/) for the development of SPM; the FMRIB Software Library laboratory at Oxford University (http://www.fmrib.ox.ac.uk/fsl) for the development of FSL; and Sergei Pakhomov, MD, Institute of the Human Brain, Russian Academy of Science, Saint Petersburg, Russia, for the development of MSU (http://www.ihb.spb.ru/~pet_lab/MSU/MSUMain.html).

References

1. DeArmond SJ, Prusiner SB. **Perspectives on prion biology, prion disease pathogenesis, and pharmacologic approaches to treatment.** *Clin Lab Med* 2003;23:1–41
2. Johnson RT, Gibbs CJ Jr. **Creutzfeldt-Jakob disease and related transmissible spongiform encephalopathies.** *N Engl J Med* 1998;339:1994–2004
3. Young GS, Geschwind MD, Fischbein NJ, et al. **Diffusion-weighted and fluid-attenuated inversion recovery imaging in Creutzfeldt-Jakob disease: high sensitivity and specificity for diagnosis.** *AJNR Am J Neuroradiol* 2005;26:1551–62
4. Shiga Y, Miyazawa K, Sato S, et al. **Diffusion-weighted MRI abnormalities as an early diagnostic marker for Creutzfeldt-Jakob disease.** *Neurology* 2004;63:443–49
5. Tofts P, ed. *Quantitative MRI of the Brain: Measuring Changes Caused by Disease.* West Sussex, UK: John Wiley; 2004
6. Kim HJ, Choi CG, Lee DH, et al. **High-b-value diffusion-weighted MR imaging of hyperacute ischemic stroke at 1.5T.** *AJNR Am J Neuroradiol* 2005;26:208–15
7. Yoshiura T, Mihara F, Tanaka A, et al. **High b value diffusion-weighted imaging is more sensitive to white matter degeneration in Alzheimer's disease.** *Neuroimage* 2003;20:413–19
8. Assaf Y, Mayzel-Oreg O, Gigi A, et al. **High b value q-space-analyzed diffusion MRI in vascular dementia: a preliminary study**. *J Neurol Sci* 2002;203–204:235–39
9. Burdette JH, Durden DD, Elster AD, et al. **High b-value diffusion-weighted MRI of normal brain.** *J Comput Assist Tomogr* 2001;25:515–19
10. **Global surveillance, diagnosis and therapy of human transmissible spongiform encephalopathies: report of a WHO consultation.** In: *Emerging and Other Communicable Diseases, Surveillance and Control.* Geneva, Switzerland: World Health Organization; 1998
11. Folstein MF, Folstein SE, McHugh PR. **"Mini-mental state": a practical method for grading the cognitive state of patients for the clinician**. *J Psychiatr Res* 1975;12:189–98
12. Chapman J, Cohen O, Nitzan Z, et al. **The CJD rating scale: a new tool for evaluation of neurologic symptomatology in early CJD patients.** *Neurology* 2007;68:A141
13. Stejskal EO, Tanner JE. **Spin diffusion measurements: spin echoes in the presence of a time dependent field gradient.** *J Chem Phys* 1965;42:288–92
14. Mukherjee P, Chung SW, Berman JI, et al. **Diffusion tensor MR imaging and fiber tractography: technical considerations.** *AJNR Am J Neuroradiol* 2008;29:843–52
15. Skare S, Andersson JL. **On the effects of gating in diffusion imaging of the brain using single shot EPI.** *Magn Reson Imaging* 2001;19:1125–28
16. Dietrich O, Heiland S, Benner T, et al. **Reducing motion artifacts in diffusion-weighted MRI of the brain: efficacy of navigator echo correction and pulse triggering.** *Neuroradiology* 2000;42:85–91
17. Mazziotta J, Toga A, Evans A, et al. **A probabilistic atlas and reference system for the human brain: International Consortium for Brain Mapping (ICBM).** *Philos Trans R Soc Lond B Biol Sci* 2001;356:1293–322
18. Ashburner J, Friston KJ. **Unified segmentation.** *Neuroimage* 2005;26:839–51
19. Brian P, Smith S, Kennedy D, et al. **FIRST: FMRIB's integrated registration and segmentation tool.** In: *Proceedings of Human Brain Mapping Conference*, June 10–14, 2007, Chicago, Illinois.
20. Fulbright RK, Hoffmann C, Lee H, et al. **MR imaging of familial Creutzfeldt-Jakob disease: a blinded and controlled study.** *AJNR Am J Neuroradiol* 2008;29:1638–43
21. Lee H, Rosenmann H, Chapman J, et al. **Thalamo-striatal diffusion reductions precede disease onset in prion mutation carriers.** *Brain* 2009 Mar 24. [Epub ahead of print]
22. Kallenberg K, Schulz-Schaeffer WJ, Jastrow U, et al. **Creutzfeldt-Jakob disease: comparative analysis of MR imaging sequences.** *AJNR Am J Neuroradiol* 2006;27:1459–62
23. Lin YR, Young GS, Chen NK, et al. **Creutzfeldt-Jakob disease involvement of rolandic cortex: a quantitative apparent diffusion coefficient evaluation.** *AJNR Am J Neuroradiol* 2006;27:1755–59
24. Tschampa HJ, Murtz P, Flacke S, et al. **Thalamic involvement in sporadic Creutzfeldt-Jakob disease: a diffusion-weighted MR imaging study.** *AJNR Am J Neuroradiol* 2003;24:908–15
25. Fulbright RK, Kingsley PB, Guo X, et al. **The imaging appearance of Creutzfeldt-Jakob disease caused by the E200K mutation.** *Magn Reson Imaging* 2006;24:1121–29
26. Nitrini R, Areza-Fegyveres R, Martins VR, et al. **Asymmetric cortical high signal on diffusion weighted-MRI in a case of Creutzfeldt-Jakob disease.** [in Portuguese]. *Arq Neuropsiquiatr* 2005;63:519–22. Epub 2005 Jul 25
27. Bavis J, Reynolds P, Tegeler C, et al. **Asymmetric neuroimaging in Creutzfeldt-Jakob disease: a ruse.** *J Neuroimaging* 2003;13:376–79
28. Wakisaka Y, Santa N, Doh-ura K, et al. **Increased asymmetric pulvinar magnetic resonance imaging signals in Creutzfeldt-Jakob disease with florid plaques following a cadaveric dura mater graft.** *Neuropathology* 2006;26:82–88
29. Yoon SS, Chan S, Chin S, et al. **MRI of Creutzfeldt-Jakob disease: asymmetric high signal intensity of the basal ganglia.** *Neurology* 1995;45:1932–33
30. Ukisu R, Kushihashi T, Tanaka E, et al. **Diffusion-weighted MR imaging of early-stage Creutzfeldt-Jakob disease: typical and atypical manifestations.** *Radiographics* 2006;26(suppl 1):S191–204
31. Ukisu R, Kushihashi T, Kitanosono T, et al. **Serial diffusion-weighted MRI of Creutzfeldt-Jakob disease.** *AJR Am J Roentgenol* 2005;184:560–66
32. Asao C, Hirai T, Yoshimatsu S, et al. **Human cerebral cortices: signal variation on diffusion-weighted MR imaging.** *Neuroradiology* 2008;50:205–11
33. Tschampa HJ, Kallenberg K, Kretzschmar HA, et al. **Pattern of cortical changes in sporadic Creutzfeldt-Jakob disease.** *AJNR Am J Neuroradiol* 2007;28:1114–18
34. Krasnianski A, Kallenberg K, Collie DA, et al. **MRI in the classical MM1 and the atypical MV2 subtypes of sporadic CJD: an inter-observer agreement study.** *Eur J Neurol* 2008;15:762–71
35. Meissner B, Kallenberg K, Sanchez-Juan P, et al. **Isolated cortical signal increase on MR imaging as a frequent lesion pattern in sporadic Creutzfeldt-Jakob disease.** *AJNR Am J Neuroradiol* 2008;29:1519–24
36. Meissner B, Kortner K, Bartl M, et al. **Sporadic Creutzfeldt-Jakob disease: magnetic resonance imaging and clinical findings.** *Neurology* 2004;63:450–56
37. Russmann H, Vingerhoets F, Miklossy J, et al. **Sporadic Creutzfeldt-Jakob disease: a comparison of pathological findings and diffusion weighted imaging.** *J Neurol* 2005;252:338–42
38. Haik S, Dormont D, Faucheux BA, et al. **Prion protein deposits match magnetic resonance imaging signal abnormalities in Creutzfeldt-Jakob disease.** *Ann Neurol* 2002;51:797–99
39. Mittal S, Farmer P, Kalina P, et al. **Correlation of diffusion-weighted magnetic resonance imaging with neuropathology in Creutzfeldt-Jakob disease.** *Arch Neurol* 2002;59:128–34
40. Mueggler T, Meyer-Luehmann M, Rausch M, et al. **Restricted diffusion in the brain of transgenic mice with cerebral amyloidosis.** *Eur J Neurosci* 2004;20:811–17
41. Brugieres P, Thomas P, Maraval A, et al. **Water diffusion compartmentation at high b values in ischemic human brain.** *AJNR Am J Neuroradiol* 2004;25:692–98
42. Clark CA, Le Bihan D. **Water diffusion compartmentation and anisotropy at high b values in the human brain.** *Magn Reson Med* 2000;44:852–59
43. Niendorf T, Dijkhuizen RM, Norris DG, et al. **Biexponential diffusion attenuation in various states of brain tissue: implications for diffusion-weighted imaging.** *Magn Reson Med* 1996;36:847–57
44. Bar-Shir A, Cohen Y. **High b-value q-space diffusion MRS of nerves: structural information and comparison with histological evidence.** *NMR Biomed* 2008;21:165–74
45. Mulkern RV, Gudbjartsson H, Westin CF, et al. **Multi-component apparent diffusion coefficients in human brain.** *NMR Biomed* 1999;12:51–62
46. DeLano MC, Cooper TG, Siebert JE, et al. **High-b-value diffusion-weighted MR imaging of adult brain: image contrast and apparent diffusion coefficient map features.** *AJNR Am J Neuroradiol* 2000;21:1830–36